GOME-2 ABSORBING AEROSOL INDEX: STATISTICAL ANALYSIS, COMPARISON TO GOME-1 AND IMPACT OF INSTRUMENT DEGRADATION

Lieuwe G. Tilstra, Olaf N.E. Tuinder, and Piet Stammes

Royal Netherlands Meteorological Institute (KNMI), Wilhelminalaan 10, De Bilt, The Netherlands

Abstract

This paper studies the Absorbing Aerosol Index (AAI) from GOME-2 as produced by KNMI within the framework of the EUMETSAT Satellite Application Facility on Ozone and Atmospheric Chemistry Monitoring (O3M SAF). The AAI is an index capable of indicating the presence of UV-absorbing aerosols. These aerosols are mainly injected into the atmosphere by desert dust and biomass burning events, but they can also originate from forest fires and volcanic eruptions. We first introduce the GOME-2 AAI to the reader, and then present the results of a validation study in which we analyse distributions of the AAI measurements. We also study time series of global means of the GOME-1 AAI and compare these with similar time series of the GOME-2 AAI. The latter time series clearly prove that the GOME-2 AAI product is suffering more and more from the effects of instrument degradation. In particular, the impact that this instrument degradation has on the AAI product is found to be very dependent on the position of the internal scan mirror of the GOME-2 instrument.

GOME-2 ABSORBING AEROSOL INDEX

The Absorbing Aerosol Index (AAI) is an index based on a comparison of measured UV reflectances with simulated Rayleigh reflectances. These simulated reflectances are calculated for cloud-free and aerosol-free atmospheres in which only Rayleigh scattering, absorption by molecules, Lambertian surface reflection as well as surface absorption can take place. The AAI is derived from another quantity, called the residue, which is defined as

$$r = -100 \cdot^{10} \log\left(\frac{R_\lambda^{obs}}{R_\lambda^{Ray}}\right) \quad (1)$$

In this equation, the superscript ^{obs} refers to reflectances measured by, in this case, GOME-2, while the superscript ^{Ray} refers to modelled Rayleigh reflectances. The symbol λ refers to the first, smallest wavelength of the wavelength pair, which is 340 nm. The surface albedo A_S used in the simulations for this wavelength is assumed to be the same as the surface albedo at the second wavelength λ_0 = 380 nm. The surface albedo at 380 nm on its turn is found from requiring that the simulated reflectance equals the measured reflectance at this wavelength. That is, we have the following two constraints:

$$R_{\lambda_0}^{obs} = R_{\lambda_0}^{Ray}(A_s) \quad ; \quad A_s(\lambda) = A_s(\lambda_0) \quad (2)$$

The two equations above basically define the algorithm that is used to calculate the residue. When a positive residue is found, absorbing aerosols were detected. Negative or zero residues on the other hand suggest an absence of absorbing aerosols. As a last step, the AAI is defined as equal to the residue where the residue is positive, and it is simply not defined for negative values of the residue.

Since November 2009 the GOME-2 AAI is an operational product in the O3M SAF. The GOME-2 level-1b data used for this paper were generated by PPF 4.0 and above. To be more specific, reprocessed level-1b data is used from 5 January 2007 to 26 June 2008 (these are data from the so-called 'R01 reprocessing'), and for the period after this date the data were taken from the regular NRT flow of level-1b PDU data products that were disseminated by EUMETSAT via EUMETCast.

The GOME-2 AAI level-2 product has a spatial resolution of 80 km by 40 km. Global coverage is achieved in 1.5 days, which makes it also quite suitable for the detection and daily monitoring of forest fires and volcanic eruptions. Figure 1 shows the GOME-2 AAI during the forest fires in central Russia in August 2010, averaged over a period of 9 days and distributed onto a latitude/longitude grid. Only the positive residues were averaged, as these alone are indicative of the presence of absorbing aerosols. Average values higher than 0.5 were considered to be caused by aerosols and plotted. The white circle indicates the position of the Russian capital Moscow, which was severely affected by the smoke from the forest fires. The extent and shape of the smoke plume agrees very well with the extent and shape of the areas of elevated levels of CO and NO_2 measured by other instruments.

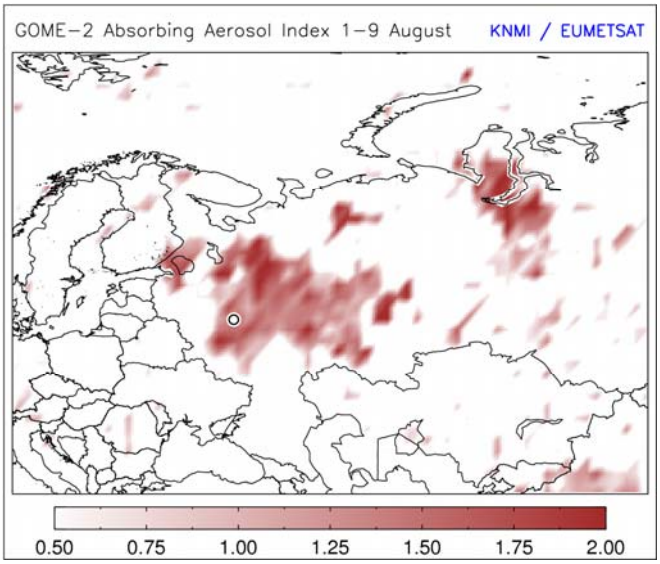

Figure 1: **Plot of the forest fires that occurred in central Russia in August 2010, as measured by the GOME-2 AAI. The positive residues, indicative of the presence of absorbing aerosols, were averaged over the period between 1 and 9 August. The white circle indicates the position of the Russian capital Moscow.**

FIRST VERIFICATION OF THE AAI

In this section we will analyse frequency distributions of residues measured by GOME-2. In Figure 2 we plotted the histogram of all residues measured by GOME-2 during the period January–April 2007 that have a latitude between 60°N and 60°S and a solar zenith angle (SZA) less than 85 degrees, that originate from the descending part of the orbit and are not part of a narrow swath or nadir static orbit, that are not affected by sunglint or solar eclipse events, and, finally, that have a “IndexInScan” number ranging between 10 and 15. These are measurements for which the viewing zenith angle (VZA) is less than 21 degrees. Here it should be added that only data with integration times of 0.375 s were taken into account, i.e., measurements of which there are 32 in each scan, and that the IndexInScan numbers mentioned are in the very middle of the forward scan (from east to west). This explains the label “NADIR” in Figure 2. The bin size of the histogram is 0.1 and data points are given by red circles. The shape of the distribution is similar to residue distributions for similar instruments like GOME-1 and SCIAMACHY, with a mean value of –0.5, a bit higher than the position of the maximum (–0.6).

As a simple verification of the absolute calibration of the AAI, we repeat the analysis, but now filter out all cloud-contaminated measurements. That is, we use the FRESCO cloud information contained inside the AAI product and apply additional filters (cloud fraction < 0.1 and cloud pressure > 800 hPa). We also expect little contamination by aerosols in the selected four months. According to the definition of the residue, for cloud-free scenes without aerosols we may expect the residue to be close to zero. The resulting histogram is given in Figure 2, using green circles. The width of the distribution has been reduced, but the position of the maximum is again found at –0.6, while we would expect to find a value close to zero. Note that the right flank of the distribution is somewhat more elevated than the left one, which is clear evidence that aerosol scenes are present and lead to positive residues.

It is hard to interpret the small deviation from zero for the mean residue of the cloud-free scenes. It may be due to remaining cloud or scattering aerosol contamination, where scattering from clouds or aerosols lowers the residue. It may also just be the result of imperfections in the model atmosphere, or it may be due to calibration errors in the reflectances. At this point it should be noted that instruments like GOME-1 and SCIAMACHY give similar (negative) values for the global mean residue of cloud-free scenes. In any case, the analysis shows that if there is an offset, it is less than 0.5 index points.

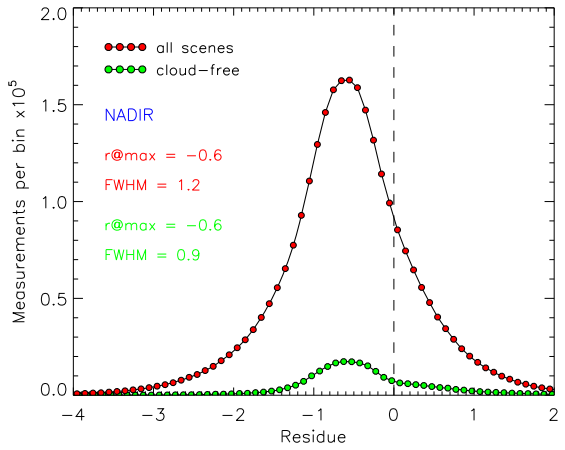

Figure 2: **Frequency distribution of the residues measured by GOME-2 for all NADIR scenes (indicated by the red circles) and cloud-free scenes (denoted by the green circles) that met the selection criteria outlined in the text.**

However, when we repeat the analysis for other parts of the GOME-2 swath, the results are somewhat different. In Figure 3 we present the results for the case in which we selected “IndexInScan” 1–6 (left window, labelled “EAST”) and “IndexInScan” 19–24 (right window, labelled “WEST”). The distribution for the eastern case clearly reaches a much lower height, which can be explained for the largest part by the filtering out of sunglint cases (which for GOME-2 are always located at the eastern side of the swath). The two distributions are also clearly more spread out, both having a FWHM of 1.7 index points. The position of the maximum for both distributions is close to zero. For the western cases, the histogram without cloud filtering seems to be deformed. The cloud-filtered distribution has a clear maximum around –0.4, in good agreement with the nadir case, and a FWHM of 0.6 index points.

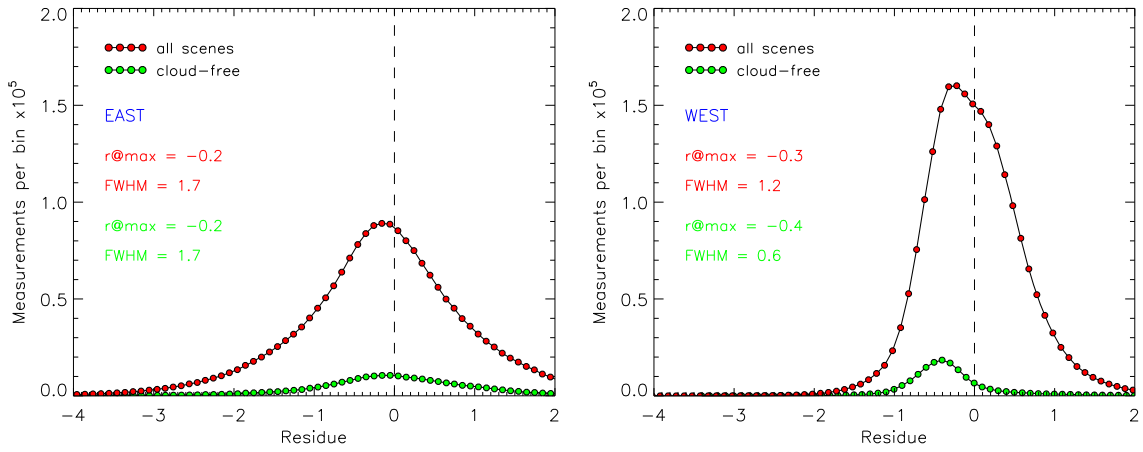

Figure 3: **Frequency distributions of the GOME-2 residues similar to the ones presented in Figure 2, but now for eastern scenes (left window) and western scenes (right window).**

In summary, the residue values are in the right range, and offset problems, if they exist, are limited to 0.5 index points. This is quite an acceptable result. The results above were found for data from the first four months of 2007, not that long after the launch of the GOME-2 instrument in October 2006. In the next section we will study the time dependence of the absolute calibration of the AAI since 2007.

GLOBAL MEAN RESIDUE

In what follows, we will analyse the global mean of residues from GOME-1 and GOME-2. Analysis of the global mean residue is a simple and robust validation technique for the AAI (see, for instance, De Graaf et al. (2005)). The global mean residue, in this report, is defined as the average of all residue measurements of a particular day that are between 60°N and 60°S and that have a solar zenith angle less than 85 degrees. It was found that sunglint situations should be excluded. They were therefore filtered out before averaging the selected residues. The same was done for data that were affected by occasional solar eclipse events. The global mean residue found in this way is more or less constant, showing only a small seasonal variation caused primarily by variation in aerosol presence.

RESULTS FOR GOME-1

In Figure 4 we present the global mean residue, as defined above, based on measurements by the GOME-1 instrument on board the ERS-2 satellite (which was launched in 1995). The time series ends in June 2003, after a permanent failure of the onboard tape recorder which prevents the satellite instrument to send all of its collected data to the ground stations. Only the three satellite footprints in the forward scan were taken into account; the backscan pixels were removed. In the first four years the global mean residue is rather stable, showing only a mild seasonal variation. This seasonal cycle is for the largest part a real one. That is, globally seen, there are more UV-absorbing aerosols (desert dust aerosol and biomass burning aerosol) in the months from May to August than there are in the months from October to January. This is clear from many publications on these types of aerosols.

The GOME-1 data that were used were intentionally not corrected for instrument degradation to illustrate the impact of instrument degradation. After an initial stable period the effects of instrument degradation start to become more and more pronounced. The global mean residue drops down by almost 5 index points, after which it oscillates back, and even reaches positive values. The situation is, however, even more complicated, because the instrument degradation is found to depend on the position of the internal scanner mirror. This is illustrated in Figure 5. Here we plotted the global mean residue for each of the three forward scan positions in each scan (East, Nadir, and West).

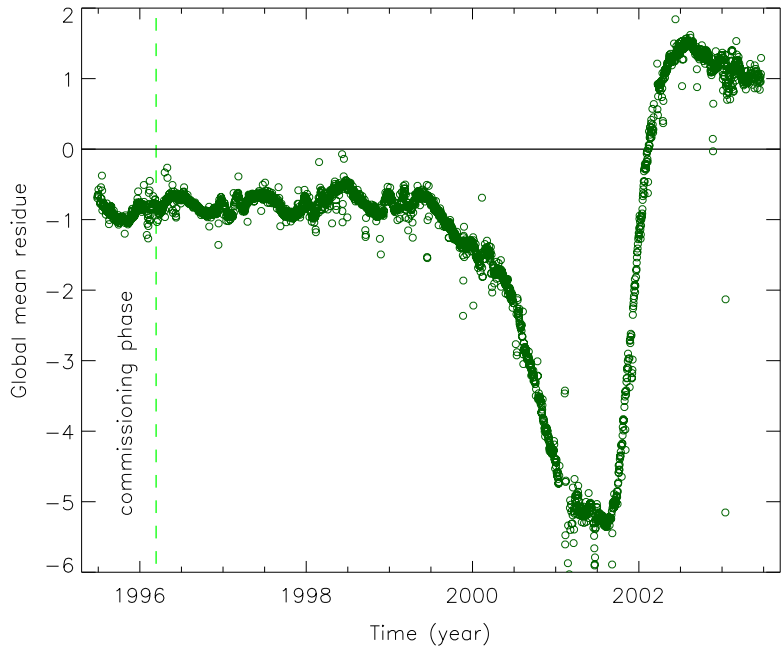

Figure 4: **Global mean residue of GOME-1 on ERS-2 as a function of time, not corrected for the effects of instrument degradation. During the first four years the global mean residue was rather stable, apart from a mild seasonal cycle. After that, instrument degradation leads to a strong decrease of the global mean residue, followed by oscillating behaviour. The time series ends on 22 June 2003, after the loss of global coverage following a tape recorder failure. The dashed vertical line indicates the end of the GOME-1 commissioning phase (12 March 1996).**

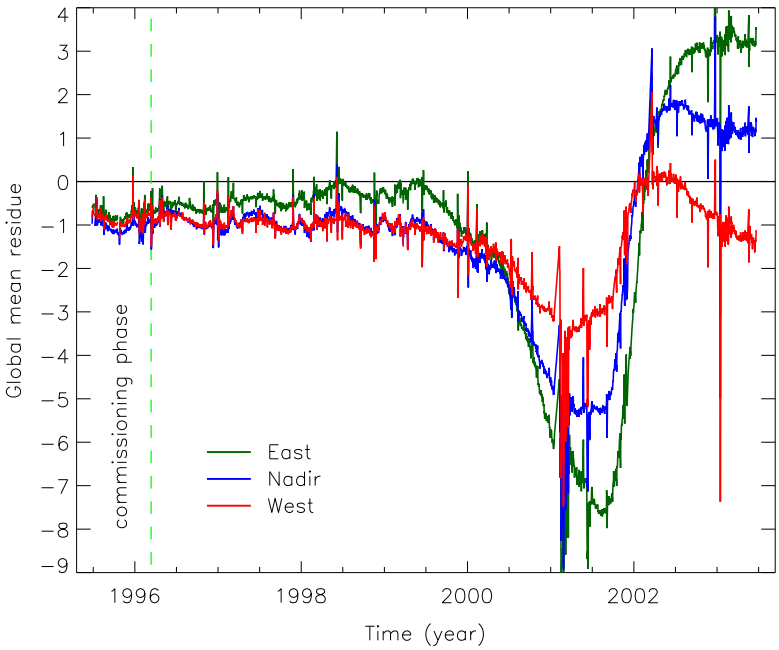

Figure 5: **Global mean residue of GOME-1 as a function of time, for each individual scan-mirror position in the forward scan of the scanning sequence (these positions are East, Nadir, and West). Again no correction for instrument degradation was applied to the data. From the plot it is clear that the impact of instrument degradation depends on the position of the scan mirror. More specifically, the west side of the swath is less affected than the east side.**

It appears from Figure 5 that the impact of the instrument degradation is the largest for the Eastern pixels, and the smallest for the Western pixels. When focusing on the first four years after launch, we see that directly after launch the global mean residues are drifting away from each other. The rate is rather low (~0.25 index point per year between East and West) and the three forward scan positions to some degree cancel each other out, which explains the initial stable period found in Figure 4. Also note the small jump at the end of the commissioning phase (indicated by the vertical dotted line) for the West pixel. During this commissioning phase the pixel size and scan mirror range were different, which has the largest impact for the pixels at the west side of the swath.

RESULTS FOR GOME-2

In Figure 6 we plotted the GOME-2 global mean residue, calculated for all days for which enough data were available. The daily averages are indicated by the black diamonds and were determined by averaging the residue values from all measurements between 60°N and 60°S that had a solar zenith angle less than 85° and that could be regarded as not affected by sunglint. Data affected by solar eclipse events were not taken into account. Furthermore, days with a low coverage as well as days containing narrow swath or nadir static orbits were removed from the time series shown in Figure 6.

The seasonal cycle reported by De Graaf et al. (2005) for the GOME-1 global mean residue is plotted in Figure 6 in the red colour. The sinusoidal curve is only a parameterisation and therefore only provides a simplified description of the real seasonal variation shown in, for instance, Figure 4. The global mean GOME-2 residue follows the seasonal behaviour of GOME-1, but it also exhibits quite a strong downward trend. Apart from that, jumps occur at several dates. These dates are indicated by the three vertical lines. The first vertical line corresponds to 11 March 2008. On this day, a new PMD band definition (v3.1) was uploaded to the satellite instrument. As a result, the global mean residue jumped up by ~0.2 index points. The second line corresponds to 18 August 2009, when a software change (from v4.2 to v4.3) occurred in the GOME-2 data processor. The global mean residue jumped down by ~0.2 index points. The third line corresponds to 9 September 2009, right in the middle of a throughput test of the GOME-2 instrument. The direct effect of this throughput test was very small.

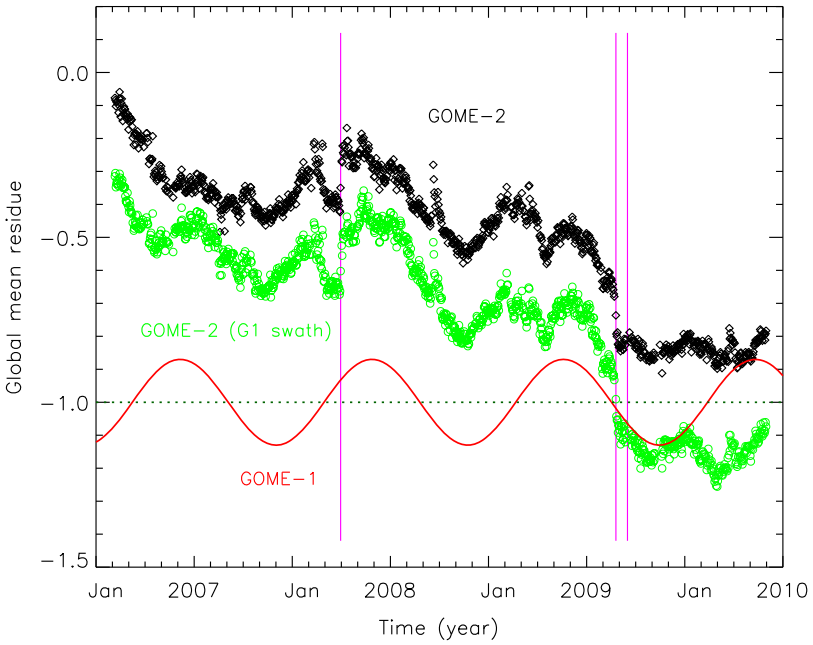

Figure 6: **Global mean residue observed by GOME-2 versus time (black diamonds). The green circles also represent the GOME-2 global mean residue, but now based only on the inner "GOME-1" part of the swath. Clearly, the data follow a seasonal cycle, and exhibit a small downward trend. For comparison, the seasonal cycle reported for GOME-1 by De Graaf et al. (2005) is also given, in red. This parameterisation is a simplification of the real seasonal cycle.**

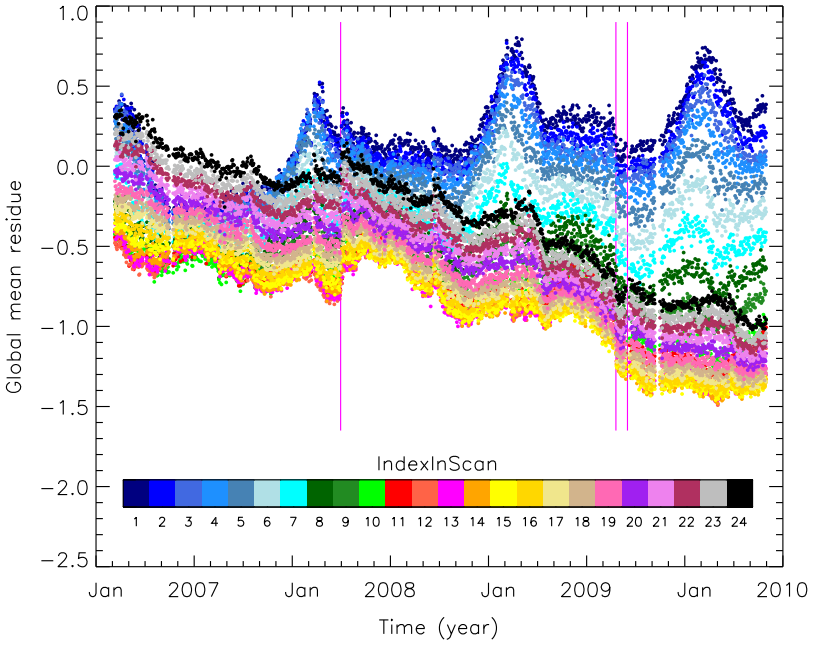

Figure 7: **Daily global mean residue for all 24 forward scan mirror positions inside the GOME-2 swath plotted versus time. The colours relate to the "IndexInScan" number, as indicated by the colour bar. There is a clear dependence on scanner angle next to the temporal variation shown before in Figure 6.**

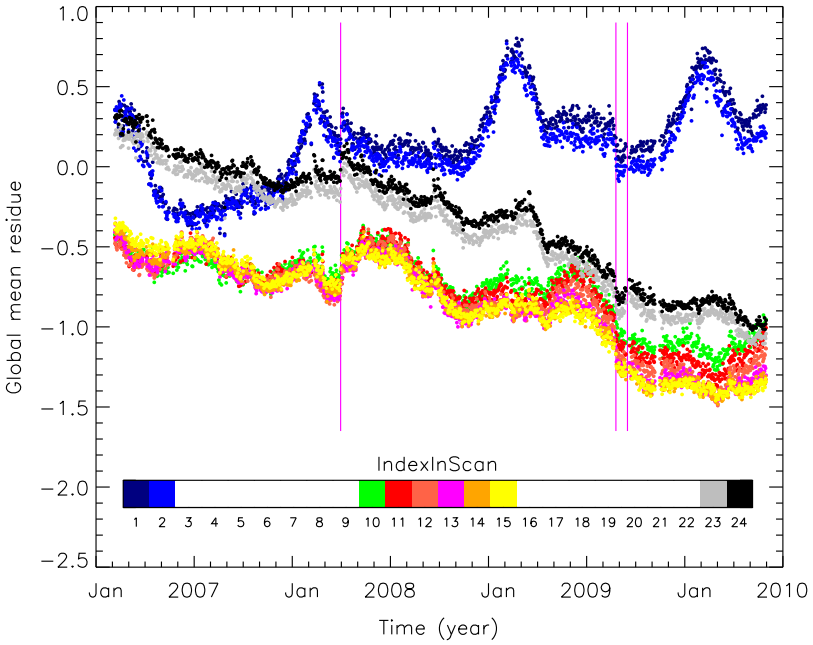

Figure 8: **Daily global mean residue versus time for a selection of the 24 forward scan mirror positions inside the GOME-2 swath. Also compare with Figure 7. The global mean residues at the east and west side of the swath are slowly drifting away from each other. The resulting east/west bias has grown to 1.5 index points.**

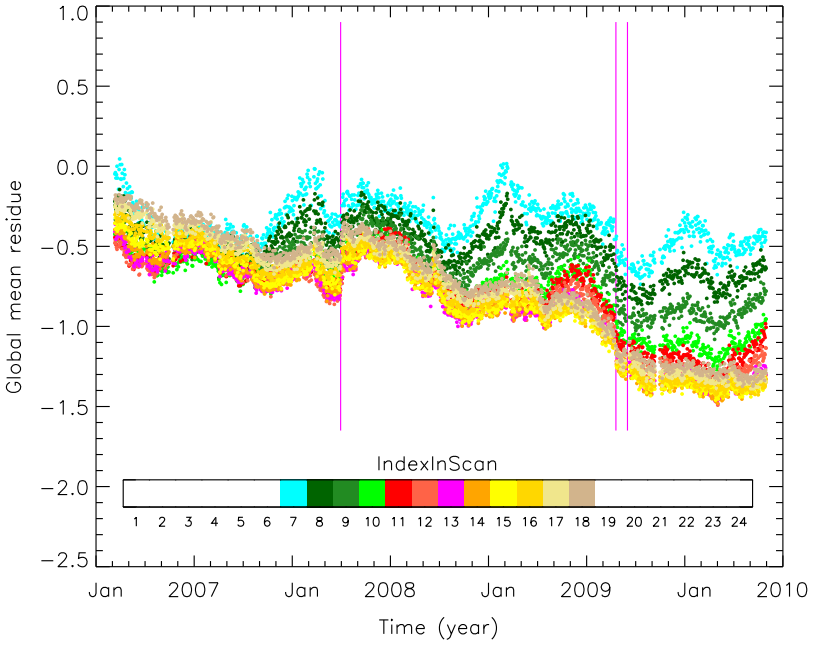

Figure 9: **Daily global mean residue versus time for another selection of the 24 forward scan mirror positions inside the GOME-2 swath. This selection of scan mirror positions corresponds to the range covered by GOME-1. The rate at which the global mean residues at the swath ends are drifting away from each other is ~0.3 index points per year.**

To investigate the effect of the wider swath of GOME-2 (1920 km) compared to GOME-1 (960 km), we also calculated the global mean residue based on the inner “GOME-1” part of the GOME-2 swath. These “small swath” results are represented in Figure 6 by the green circles. Their behaviour is similar to the “full swath” behaviour, but the values are lower and therefore closer to the GOME-1 result. Note that the differences between the “small swath” and “full swath” result are increasing with time. The latter behaviour is directly pointing to scan-angle dependent instrument degradation.

In Figure 7 we therefore present the daily global mean residue versus time for all the individual forward scan mirror positions. There are 24 measurements inside each forward GOME-2 scan, resulting in 24 time series, each with their own colour and labelled by their own “IndexInScan” number. The general behaviour for each of the scanner mirror positions is similar to that presented in Figure 6, but there is also a clear difference in offset. Also, the value of the global mean of one scanner angle relative to those of the other scanner angles is varying. This is more clearly shown by Figure 8, which differs from Figure 7 in the sense that only data for a selection of scan mirror positions is plotted. The westernmost scanner mirror position (given in black) shows a significantly different temporal behaviour than the easternmost scanner mirror position (given in dark blue). More importantly, at the start of the time series, the easternmost and westernmost scanner mirror positions show exactly the same value for the global mean residue. But more than three years later, the difference has increased to roughly 1.5 index points. After the same period of time, however, GOME-1 showed only a very mild east/west bias of ~0.8 index points, as can be concluded from Figure 5.

The large east/west bias as compared to GOME-1 in its first four years is partly caused by the simple fact that the swath width of GOME-2 is twice the swath width of GOME-1 (1920 km versus 960 km). To illustrate this, we present in Figure 9 again the GOME-2 global mean residue, but now for the inner part of the GOME-2 swath. For these more nadir-viewing geometries, the temporal behaviour is less wild, and the east/west bias, caused by instrument degradation, is also less: 1.0 index points, somewhat larger than the 0.8 index points found for GOME-1 roughly 3.5 years after its launch. We therefore conclude that the GOME-2 instrument is suffering somewhat more from reflectance degradation than its predecessor GOME-1, but that the degradation pattern so far is very similar.

CONCLUSIONS

The GOME-2 AAI studied in this paper is found to behave as it should. Frequency distributions of the AAIs are very similar to those obtained from other instrument, like GOME-1 and SCIAMACHY. A possible offset was found, but it is very small (<0.5 index points) so that it cannot be determined if the offset is real (due to errors in the radiometric calibration of the reflectance), or just a result of the inaccuracy of the methods we used for verification.

Like other satellite instruments, GOME-2 is suffering from optical degradation. We presented analyses of the global mean residue of GOME-2 and of its predecessor, GOME-1. Both instruments are affected by scan-angle dependent instrument degradation, resulting in a downward trend in the global mean residue and a growing east/west bias. However, GOME-2 is more affected than GOME-1 in its lifetime, which for the largest part can be explained by the larger range covered by the scan mirror. If GOME-2 continues to follow a similar pattern of instrument degradation as GOME-1, then a very dramatic drop in the AAI values should occur within in the next two years.

In conclusion, the results indicate that the GOME-2 AAI is of good quality, but that optical instrument degradation is severely affecting the quality already right from the start of the time series. It is therefore essential for maintaining the quality of the AAI product to develop (in the near future) a correction for instrument degradation that can be applied to the Earth reflectance measurements.

REFERENCES

De Graaf, M., Stammes, P., Torres, O., Koelemeijer, R.B.A., (2005) Absorbing Aerosol Index: Sensitivity analysis, application to GOME and comparison with TOMS, J. Geophys. Res., **110**, doi:10.1029/2004JD005178